*Article*

# Photocatalytic Degradation of Valsartan by MoS$_2$/BiOCl Heterojunctions

**Eleni Grilla [1], Maria Nefeli Kagialari [1], Athanasia Petala [1], Zacharias Frontistis [2] and Dionissios Mantzavinos [1,*]**

[1] Department of Chemical Engineering, University of Patras, Caratheodory 1, GR-26504 Patras, Greece; elen.grilla@gmail.com (E.G.); nefkg97@gmail.com (M.N.K.); natpetala@chemeng.upatras.gr (A.P.)

[2] Department of Chemical Engineering, University of Western Macedonia, GR-50150 Kozani, Greece; zfrontistis@uowm.gr

[*] Correspondence: mantzavinos@chemeng.upatras.gr; Tel.: +30-261-099-6136; Fax: +30-261-099-1527

**Abstract:** In the present study, the removal of valsartan (VLS), an antihypertensive agent, under simulated solar radiation with the use of molybdenum sulfide-bismuth oxychloride composites (MoS$_2$/BiOCl), of variable MoS$_2$ content (0.1–10.0 wt.%) was investigated. The physicochemical properties of the photocatalysts were examined by XRD, DRS, BET and TEM/HRTEM. Preliminary tests were conducted to examine the photocatalytic efficiency of the synthesized MoS$_2$/BiOCl composites towards VLS degradation in ultrapure water (UPW). It was found that the activity of pure BiOCl is improved with the addition of MoS$_2$. The degradation rate was maximized with the use of the catalyst containing 0.25 wt.% MoS$_2$. It was also found that the increase in catalyst concentration (50–1000 mg/L) enhances VLS degradation. It was found that VLS removal decreased by increasing VLS concentration. The effect of the water matrix on VLS removal was studied by carrying out experiments in real and synthetic water matrices. VLS degradation in UPW was faster than in bottled water (BW) and wastewater (WW), mainly due to the existence of organic matter in real aqueous media. Lastly, 0.25 wt.% MoS$_2$/BiOCl showed great stability after 360 min of irradiation, serving as a promising catalyst for water remediation of emerging contaminants under solar irradiation.

**Keywords:** bismuth oxychloride; antihypertensive; valsartan; water matrix; photocatalysis

## 1. Introduction

The ubiquity of pharmaceutically active compounds (PhACs) in aqueous media is one the biggest topics of concern for the 21st century [1–3]. PhACs mainly end up in waters through direct uncontrolled discharge from hospitals, households and industries, as well as through excretion from humans and animals' faeces or urine [2,3].

According to some studies, antihypertensive compounds are one of the PhACs groups that have high total average concentration in influent wastewaters. One of the compounds that is frequently prescribed is VLS, which is a highly selective and orally active Angiotensin II receptor antagonist (ARA-II) for hypertension and heart failure treatment [4,5]. VLS is mainly recovered in faeces and urine when given as an oral solution. Approximately 20% of the dose is recovered as metabolites, so the recovery is more as an unchanged compound [6]. There have been reports of its presence in wastewater treatment plants all over the world, at concentrations between 11 ng/L and 6 µg/L [7–10]. These levels prove VLS minor degradation by conventional wastewater treatments plants. Therefore, alternative treatments need to be developed to remove VLS from waters.

Advanced oxidation processes (AOPs) can be a viable choice for the elimination of compounds of this type, as they have shown a great potential in treating pollutants of low or high concentration of organic compounds [11,12]. These technologies are based on hydroxyl radical (·OH) production, which can be activated by ozone, hydrogen peroxide, heat, etc. These radicals are highly reactive and can oxidize a large number of organic

compounds [13]. Within the AOPs, semiconductor photocatalysis has demonstrated its ability to decompose a great variety of PhACs from water and wastewater [14,15]. Most researchers have focused on titanium dioxide ($TiO_2$)-based catalysts, since $TiO_2$ possesses the majority of the desirable features of a photocatalyst—low cost, high stability and zero toxicity [16]. However, due to its wide bandgap (3.0–3.2 eV) it is active only under UV radiation. As a result, researchers have concentrated their efforts on developing photocatalysts that achieve maximum photocatalytic activity in the full range of the electromagnetic spectrum, the solar system [17].

Bismuth-based materials have attracted considerable attention for organic dyes and especially PhACs degradation under visible light irradiation [18]. For instance, promising results came by using bismuth vanadate ($BiVO_4$) for the removal of both organic dyes and antibiotics [19–21]. However, despite its low bandgap (2.4 eV), low toxicity and low cost [22], $BiVO_4$ suffers from excessive electron-hole recombination [23]. Moreover, bismuth oxyhalides (BiOCl, BiOI and BiOBr), have shown high performance in different photocatalytic configurations [24–26]. Among them, BiOCl, due to its layered structure, has an internal electrostatic field, resulting in the successful separation of photogenerated electron-hole pairs [27–30]. As a result, it has been successfully adopted as photocatalyst in many studies [27–30]. For example, Zhang et al. [24] used BiOCl to degrade methyl orange (MO) dye, showing superior performance than $TiO_2$ (P25). However, its large band gap energy (3.2 eV) restricts its activity only under UV light [27–30]. In order not only to extend BiOCl's visible light harvesting properties, but also to enhance its photocatalytic activity, researchers have proposed many morphological and structural modifications [31–33]. Zang et al. prepared a Z-scheme $Ag/BiOCl/AgIO_3$ heterojunction, characterized by desired electronic properties, showing higher rhodamine B degradation rate than pure BiOCl [31]. In a similar manner, a heterogeneous doped interface Ta-BiOCl/Bi also showed improved catalytic activity for the elimination of both rhodamine B and tetracycline compared to Ta-BiOCl, BiOCl/Bi and BiOCl [32]. Moreover, the photodegradation of ciprofloxacin was greatly enhanced using PVP-induced $Bi_2S_3/BiOCl$ heterostructures [33]. In other studies, Bao et al. [34] reported that $BiOCl/TiO_2$ was an efficient photocatalyst to degrade antibiotics under visible-light irradiation.

Molybdenum disulfide ($MoS_2$) is a silver black solid that is similar to graphite and has attracted researchers' enthusiasm in recent years [35,36]. $MoS_2$, with a narrow band gap (1.3–1.8 eV), is a promising two-dimensional material which demonstrates large surface area and high electrical conductivity, implying that it could be used as a suitable catalyst support [37,38]. Until now, no report has discussed the application of BiOCl combined with $MoS_2$ in the degradation of pharmaceuticals, but only in common dyes, such as rhodamine B [35,39].

In this respect, this work investigates the heterojunction structure between $MoS_2$ and BiOCl as a promising photocatalyst in the elimination of VLS under solar radiation. Issues associated with the effect of catalyst composition, stability and process parameters, including catalyst concentration, type of irradiation, initial pH solution, the quality of actual and synthetic water matrices on VLS degradation are also studied.

## 2. Results

### 2.1. Catalyst Characterization

Figure 1 shows the XRD patterns of pure BiOCl and $MoS_2$ samples as well as of the composite $MoS_2/BiOCl$ photocatalysts. For BiOCl, the diffraction peaks can be indexed to the well-crystallized tetragonal phase of BiOCl (JCPDS 6-249), in accordance with previous studies [35,39]. Specifically, the peaks located at 24.2°, 32.5°, 33.6°, and 46.8° are, respectively, indexed to (002), (110), (102), and (200) crystal planes of tetragonal BiOCl. It is observed that with the addition of $MoS_2$ to these peaks gradually became less sharp, indicating that the primary crystallite size becomes smaller. These phenomena are more evident for the samples containing 1 and especially 10 wt.% $MoS_2$. The primary crystallize size of the synthesized photocatalysts are shown on Table 1. It is observed that crystallite

size reduces from 26 nm for pure BiOCl to 10 nm for 10 wt.% MoS$_2$/BiOCl. The XRD pattern of pure MoS$_2$ matches well with the JCPDS card 9-312 for MoS$_2$ and its crystallite size was found to be equal to 1 nm. Table 1 also presents the specific surface area of all samples. It appears that specific surface area of BiOCl increases with the addition of MoS$_2$. Zeta potential measurements (Figure 1B) revealed that the 0.25 wt.% MoS$_2$/BiOCl surface is negatively charged throughout pH scale. In addition, at more basic conditions, the negative charge increased.
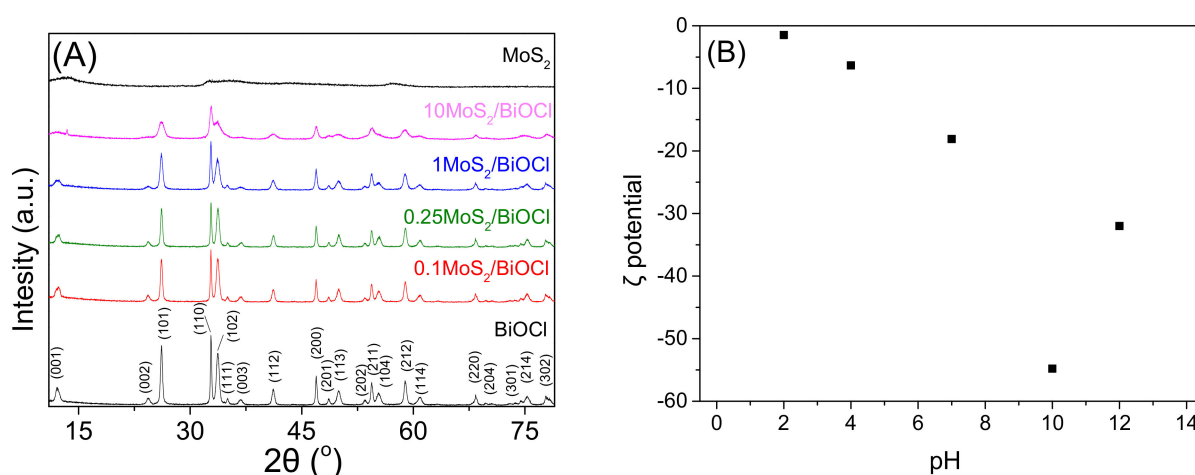


**Figure 1.** (**A**) X-ray diffraction patterns obtained for pure BiOCl and MoS$_2$/BiOCl photocatalysts. (**B**) Zeta potential of 0.25 wt.% MoS$_2$/BiOCl as a function of pH.

**Table 1.** Characterization of the synthesized catalysts.

| Samples | Primary Crystallize Size, nm | SSA, m$^2$/g |
|---|---|---|
| 10 wt.% MoS$_2$/BiOCl | 10 | 38 |
| 1% wt.% MoS$_2$/BiOCl | 19 | 27 |
| 0.25% wt.% MoS$_2$/BiOCl | 26 | 20 |
| 0.1% wt.% MoS$_2$/BiOCl | 26 | 18 |
| BiOCl | 26 | 21 |

Figure 2A,B presents characteristic TEM images of BiOCl. It is observed that BiOCl consists of nanoplates with diameter ranging from 42 to 125 nm with average thickness equal to ~13 nm. It is interesting to note (Figure 2B) that the edges of the nanoplates are made up of very small spheres. The addition of MoS$_2$ (Figure 2C,D) does not seem to bring about significant changes in the morphology of BiOCl. However, small spherical nanoparticles with an average diameter equal to ~3 nm are evident all over the surface of BiOCl. HRTEM images can provide a clearer view of the material structure by measuring the identified intra-atomic distances. Considering pure BiOCl (Figure 2E), the lattice spacing of 0.34 nm corresponding to the (101) plane of BiOCl prevails. After the addition of MoS$_2$ (Figure 2F), no additional lattice spacings could be observed; however, at the BiOCl surface, small spherical particles can be observed, probably attributed to MoS$_2$, due to its low crystallinity.
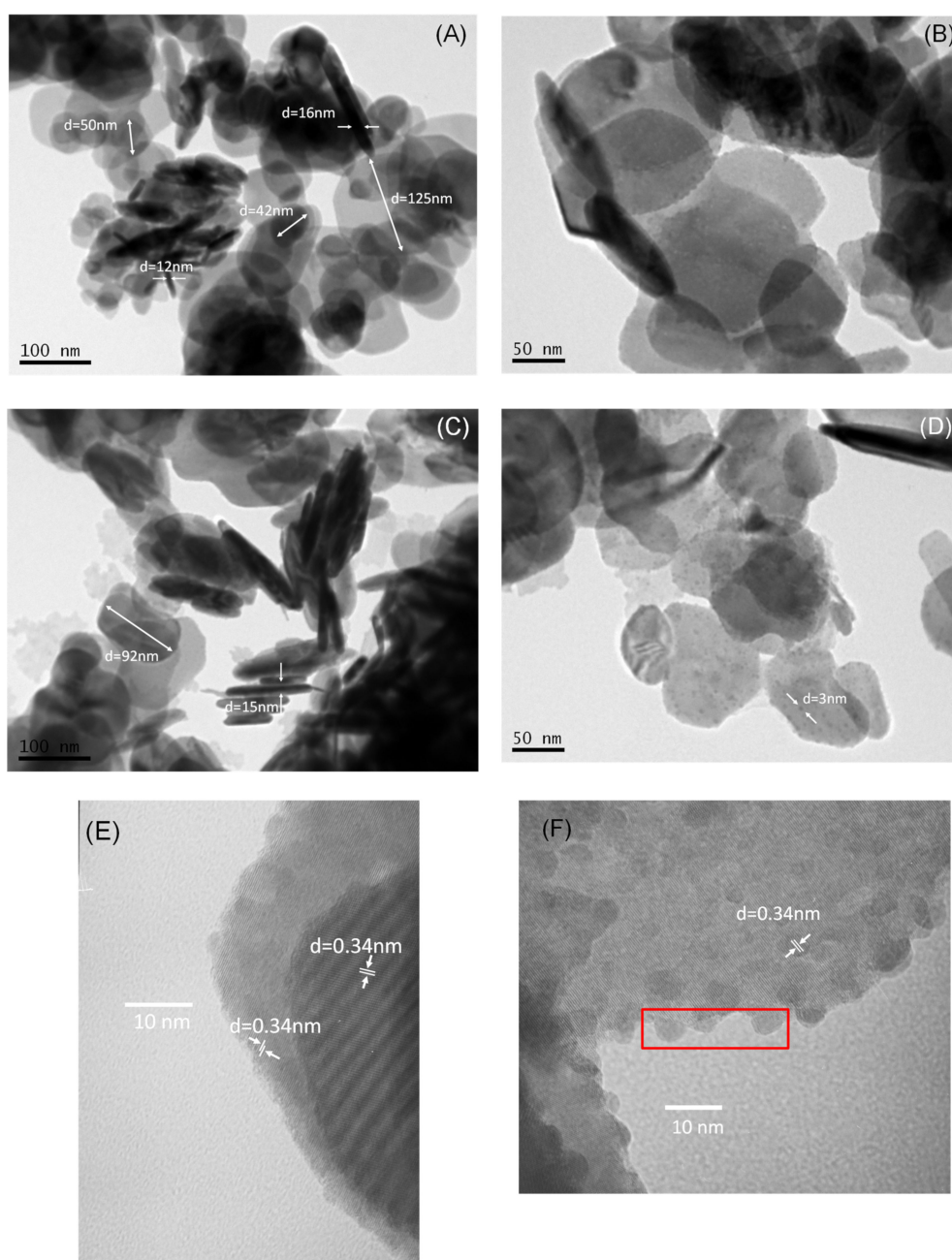
**Figure 2.** TEM images of (**A**), (**B**) BiOCl and (**C**), (**D**) 0.25 wt.% $MoS_2$/BiOCl at different magnifications. HRTEM images of (**E**) BiOCl and (**F**) 0.25 wt.% $MoS_2$/BiOCl.

UV–visible diffuse reflectance spectroscopy was adopted in order to investigate the optical properties of all the synthesized materials (Figure 3A). It is observed that BiOCl has an absorption threshold at $\lambda$ ~450 nm, which remains practically intact after the addition of relatively small quantities of $MoS_2$. However, 10 wt.% $MoS_2$/BiOCl sample is characterized by improved absorption at the visible part of the solar spectrum. Furthermore, the band gap of the photocatalysts was defined from Tauc plots (Figure 3B). The pure BiOCl band gap was found to be equal to 2.5 eV, in accordance with previous studies [39]. Moreover, despite the fact that composite samples show greater absorption in higher wavelengths, their band gap value is not practically altered after $MoS_2$ addition.
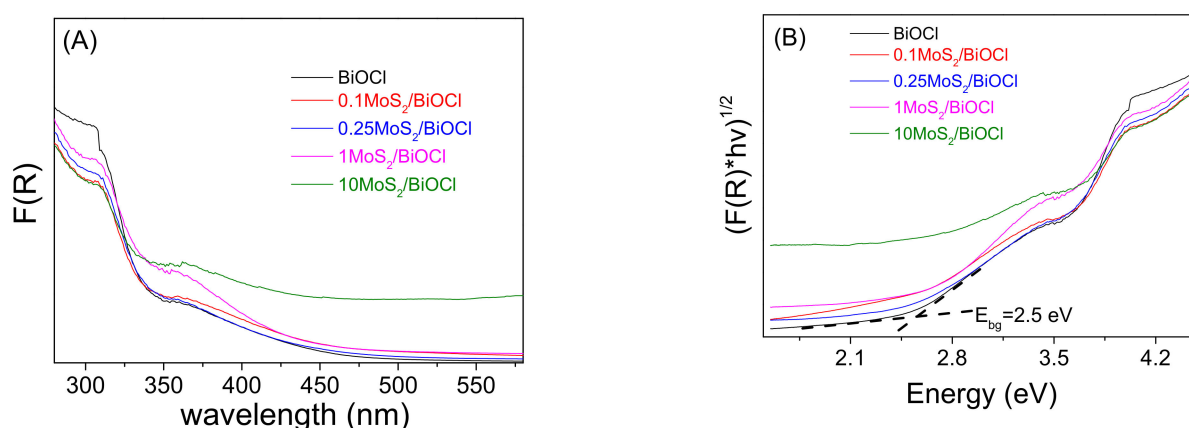
**Figure 3.** (**A**) UV–vis diffuse reflectance spectra obtained for for pure BiOCl and MoS$_2$/BiOCl photocatalysts. (**B**) Tauc plot obtained from the DRS spectrum.

### 2.2. Catalyst Activity

Preliminary tests were carried out to evaluate the photocatalytic activity of BiOCl and to examine whether the heterojunction of BiOCl with MoS$_2$ could improve its photocatalytic activity for VLS removal in ultrapure water (UPW) under simulated solar irradiation. Experiments were conducted at 1000 mg/L catalyst concentration. As seen from Figure 4a, the addition of small amounts of MoS$_2$ up to 0.25 wt.% increases the photocatalytic activity of BiOCl; complete degradation of VLS was observed after 60 min, where only 80% VLS was degraded at the same time in the case of pure BiOCl. However, a further increase in the amount of MoS$_2$ results in a decrease in VLS degradation rate. The best outcomes were confirmed for the catalyst loaded with 0.25 wt.% MoS$_2$, where 0.5 mg/L VLS was degraded after 60 min. It is worth mentioning that photolysis alone does not participate to VLS degradation, as only 10% 0.5 mg/L VLS was degraded after 60 min. To estimate reaction rates, the degradation of VLS is considered to follow a pseudo-first order kinetic expression, (Equation (1)) [40]:

$$-\frac{dC}{dt} = kC \Rightarrow \ln\left(\frac{C_0}{C}\right) = k_{app}t \tag{1}$$

where C and C$_0$ is VLS concentration at time t = t and t = 0, respectively, and k$_{app}$ is an apparent rate constant incorporating the relatively constant concentration of oxidizing species.
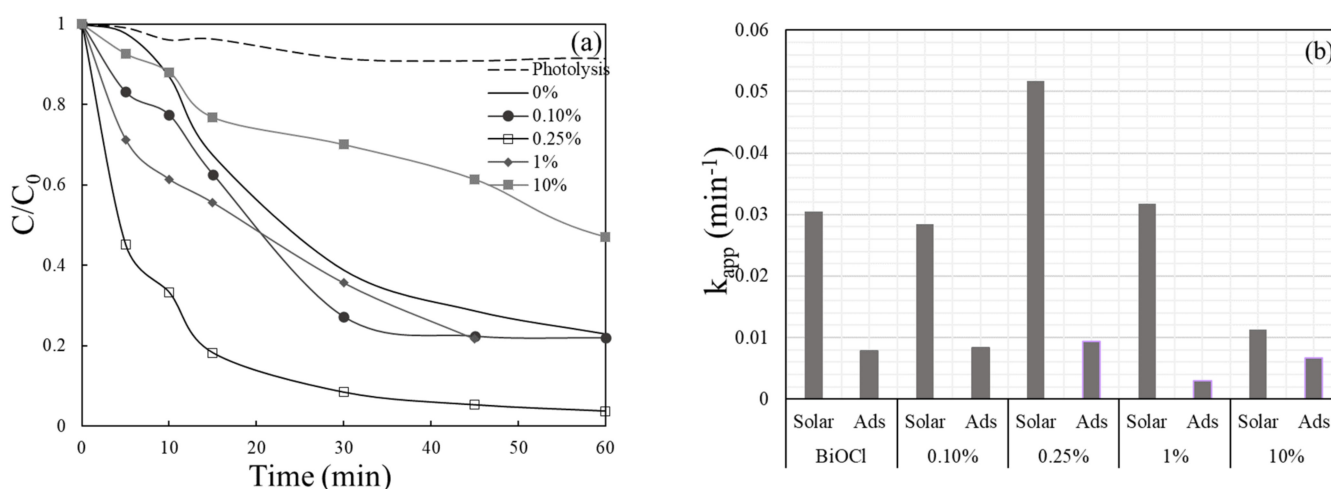


**Figure 4.** (**a**) Photocatalytic activity of 1000 mg/L BiOCl and MoS$_2$/BiOCl composites for the degradation of 0.5 mg/L VLS in UPW. (**b**) Relationship between apparent rate constant and the different composites of the synthesized catalyst.

The computed apparent constant rates are shown in Figure 4b. In the same Figure adsorption results (in the absence of irradiation) for each case are also presented. In view of these results, the rate constants corresponding to 0.1 $MoS_2$/BiOCl, 0.25 $MoS_2$/BiOCl, 1 $MoS_2$/BiOCl, 10 $MoS_2$/BiOCl and pure BiOCl for the degradation of VLS are calculated as 0.0284, 0.0517, 0.0318, 0.0113 and 0.0305 $min^{-1}$, respectively, indicating that 0.25 $MoS_2$/BiOCl composite has the highest degradation performances.

As demonstrated in Scheme 1, photogenerated electrons and holes are produced over BiOCl and $MoS_2$ under solar irradiation. Because of the relative position of their conduction (CB) and valence band (VB), when making contact, electrons will be moved to the CB of BiOCl, and holes will be transferred in the VB of $MoS_2$ [39,41]. At the same time, p–n heterojunctions are created at the interfaces of the p-type $MoS_2$ and the n-type BiOCl semiconductors, thus hindering their recombination [42,43]. Photogenerated species can now start redox reactions for VLS degradation. VLS can be oxidized directly by photogenerated holes, while photogenerated electrons reduce absorbed $O_2$ resulting in the formation of more reactive species (i.e., superoxide anions) which can also contribute to VLS oxidation.
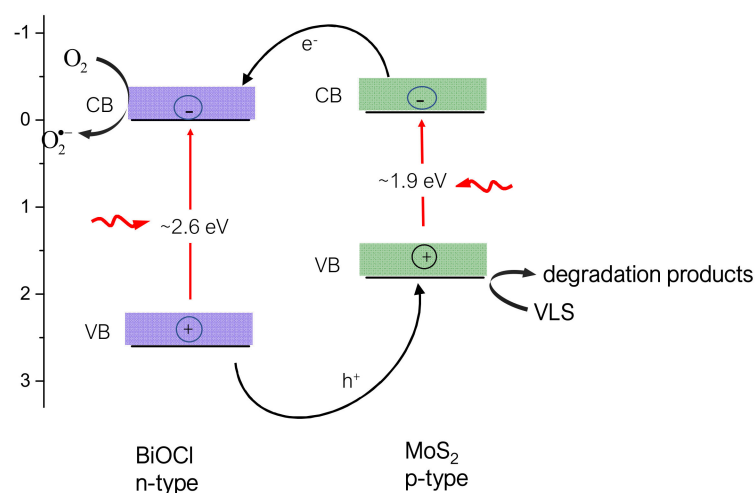


**Scheme 1.** Simplified diagram showing the relative band edge positions and charge separation in irradiated $MoS_2$/BiOCl photocatalyst.

## 2.3. Effect of Operating Conditions

VLS degradation as a function of rising catalyst loading in the range 50–1000 mg/L is shown in Figure 5. It is observed that increasing catalyst concentration VLS degradation increases, with complete degradation achieved after 60 min of irradiation at 1000 mg/L 0.25 $MoS_2$/BiOCl, confirming the relationship between the photocatalyst sites available for reaction and the degradation rate [44].

The impact of changing initial VLS concentration between 0.25 mg/L and 1 mg/L on its destruction is shown in Figure 6. As it can be seen, VLS degradation rises with decreasing its initial concentration. For example, 77% removal occurs after 15 min of irradiation at 0.25 mg/L concentration and 82%, 22% at 0.5 and 1 mg/L, respectively. The computed apparent rate constants are 0.1003, 0.0517 and 0.0138 $min^{-1}$ at 0.25, 0.5 and 1 mg/L initial concentrations of VLS, which implies that the reaction is not true first order since the rate alters with concentration and the data fit to Equation (1). The concentration of reactive species becomes the limiting reactant as VLS concentrations rise, explaining the observed near-zeroth order kinetics. [40].
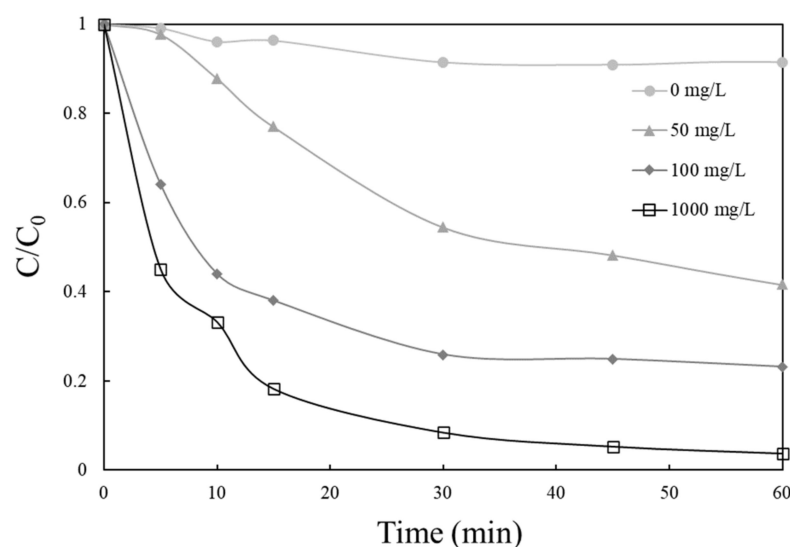
**Figure 5.** Effect of the catalyst concentration of 0.25 $MoS_2$/BiOCl on the degradation of 0.5 mg/L VLS under simulated solar irradiation in UPW.
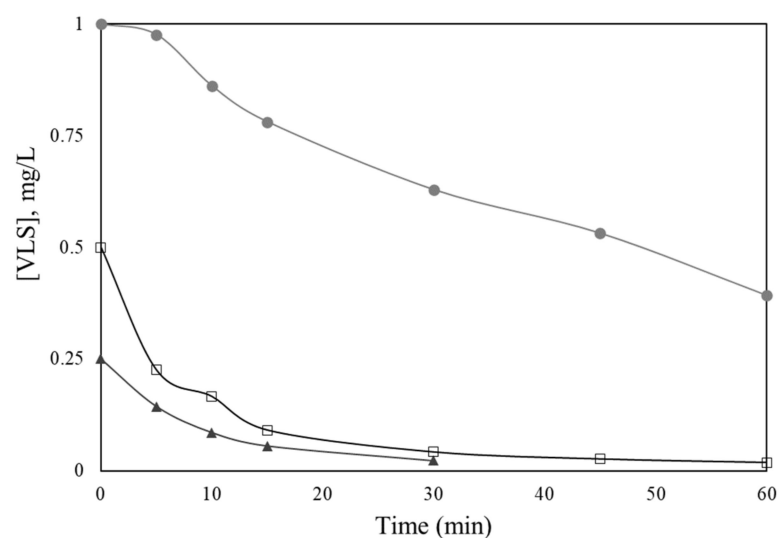


**Figure 6.** Effect of VLS concentration on its degradation with 1000 mg/L 0.25 $MoS_2$/BiOCl in UPW under solar irradiation.

Additional tests were performed to find out if the type of irradiation affects the destruction of 0.5 mg/L VLS in the presence of 1000 mg/L 0.25 $MoS_2$/BiOCl, and results are presented in Figure 7. After 60 min of irradiation, 70% and 30% removal of VLS was achieved under UV and visible irradiation, respectively, showing that, under solar irradiation, VLS degradation occurs to a significant extent, with $k_{app}$ = 0.0517 min$^{-1}$, which is 4 times higher than $k_{app}$ = 0.0131 min$^{-1}$ under UV irradiation. As a result, the ultraviolet portion of the solar spectrum tends to have a significant impact on VLS degradation.

To explore the photocatalytic activity of 0.25 $MoS_2$/BiOCl in various water matrices, experiments were performed in actual and synthetic matrices, including WW, commercially available BW and UPW spiked with HA, chloride and bicarbonate compounds and the results are summarized in Figure 8. HA was chosen to simulate the organic matter found in natural waters, in concentrations that match the organic compound of real water matrices in inherent pH. As seen in Figure 8a, degradation in WW and in BW is entirely blocked, confirming that the organic and inorganic constituents of WW and BW compete fiercely with VLS for the catalyst's reactive species. However, when a mixture containing the amounts of bicarbonates and chlorides that comprise commercially available BW, was

added in UPW, an enhanced behaviour on the degradation of VLS compared to BW observed, implying that probably the presence of organic matter restricts the degradation rate. To confirm this assumption, additional tests were carried out in UPW with different concentrations of HA, sodium bicarbonate and sodium chloride, and the results, expressed as apparent kinetic constants, are given in Figure 8b. Indeed, the addition of HA has a negative impact on removal rate; the rate decreases as HA concentration increases, while no considerable effect was seen when chloride ions ($Cl^-$) was added in UPW at 50–150 mg/L. In contrast, it seems that bicarbonates alone, at low concentration (30 mg/L), has a positive effect on VLS removal. Bicarbonate and carbonate ions ($HCO_3^-$, $CO_3^{2-}$) are usually assumed to decrease photocatalysis efficiency by scavenging ·OH and forming carbonate radicals, which is characterized by lower oxidation potential ($E° = 1.78$ V at pH = 7) than ·OH ($E° = 2.3$ V at pH = 7) [45]. Carbonate radicals, on the other hand, are considered more stable and they have a longer lifetime than ·OH, so they can disperse away from the catalyst surface and react with organic molecules in the liquid bulk rapidly [46]. As a result, the organic constituents of the WW matrix, as well as the presence and scavenging behaviour of the WW matrix unknown constituents, may have a negative impact on VLS degradation.
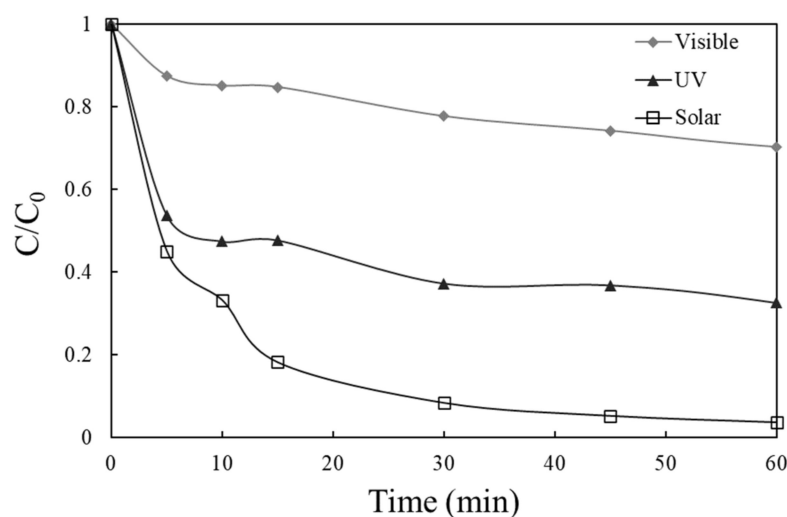


**Figure 7.** Effect of the type of irradiation on 0.5 mg/L VLS degradation with 1000 mg/L 0.25 $MoS_2$/BiOCl in UPW.
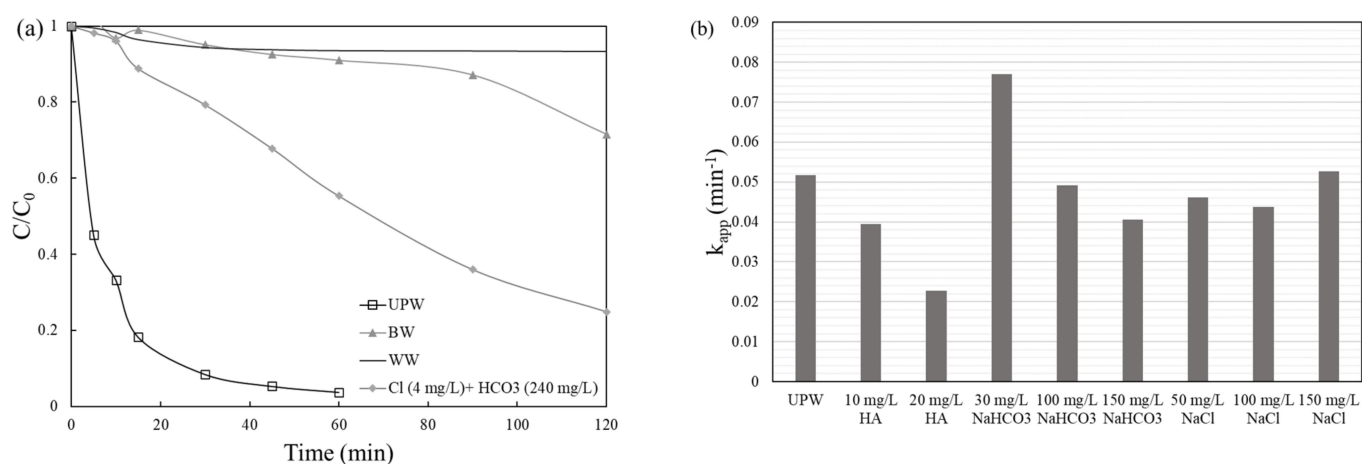


**Figure 8.** (**a**) Effect of water matrix on 0.5 mg/L VLS degradation with 1000 mg/L 0.25 $MoS_2$/BiOCl under solar irradiation. (**b**) Constant apparent rates of the degradation of 0.5 mg/L VLS in UPW spiked with different constituents.

Additional tests were conducted to assess the impact of initial pH values on 0.5 mg/L VLS decomposition. The inherent value of 5.5 in UPW was adjusted to acidic (pH = 3.1) and basic (pH = 9.7) conditions and results are depicted in Figure 9. As it can be observed, after 60 min of irradiation VLS was degraded at inherent pH, while only 60% VLS was degraded under acidic and basic conditions. Moreover, at acidic and basic conditions computed constant rates was decreased at 0.0155 and 0.0144 min$^{-1}$, respectively. The observed reduced SMX removal in basic environment could be associated with the growing electrostatic repulsion between 0.25 MoS$_2$/BiOCl and SMX since both are negatively charged. This is verified by photocatalyst's zeta potential measurements (Figure 1B), showing its surface negative charge at pH > 9. On the other hand, under acidic conditions, electrostatic attraction would be expected to lead to improved SMX degradation. The fact that this was not observed is probably due to catalyst dissolution at acidic pH.
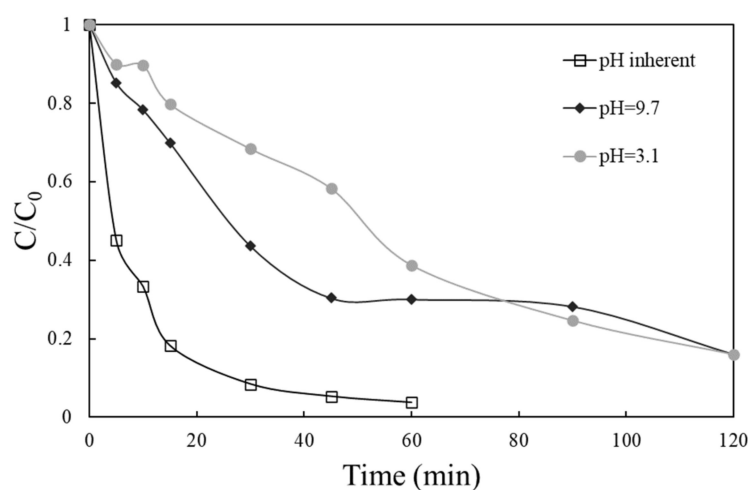


**Figure 9.** Effect of initial pH solution on the degradation of 0.5 mg/L VLS with 1000 mg/L 0.25 MoS$_2$/BiOCl in UPW.

### 2.4. Mechanism of VLS Degradation and Catalyst Reusability

Additional experiments were carried out using scavengers, such as t-butanol and EDTA, at concentrations higher than VLS, with the results shown in Figure 10. The addition of tert butanol (2.5 g/L), which acts as an ·OH scavenger, appears to have little impact on VLS destruction. In the presence of EDTA, a well-known hole scavenger; however, the degradation is quenched [47], indicating that the most active species for the photocatalytic degradation of VLS are the photogenerated hole. This result came to an agreement with previous studies, using EDTA as a scavenger [35]. Therefore, it is justifiable to assume that h$^+$ active species plays the most crucial role in the degradation procedure. These findings are in accordance with the proposed photocatalytic degradation mechanism (Scheme 1), where it is shown that the VB of MoS$_2$ is located at +1.81 V vs. NHE, while the potential of ●OH formation is 2.38 V vs. NHE, thus not allowing their formation.

The catalytic activity of 0.25 MoS$_2$/BiOCl upon repeated use for the degradation of 0.5 mg/L VLS was explored in a final series of experiments. The reaction mixture was exposed to irradiation for 90 min, after which the residual VLS concentration was determined. Then, the reactor was re-loaded up to 0.5 mg/L VLS and further irradiated for 90 min. Figure 11 shows the outcome of repeating this cycle twice. The extent of VLS degradation was near 90% for all four cycles, showing that this catalyst exhibits excellent stability on the photocatalytic degradation of VLS.
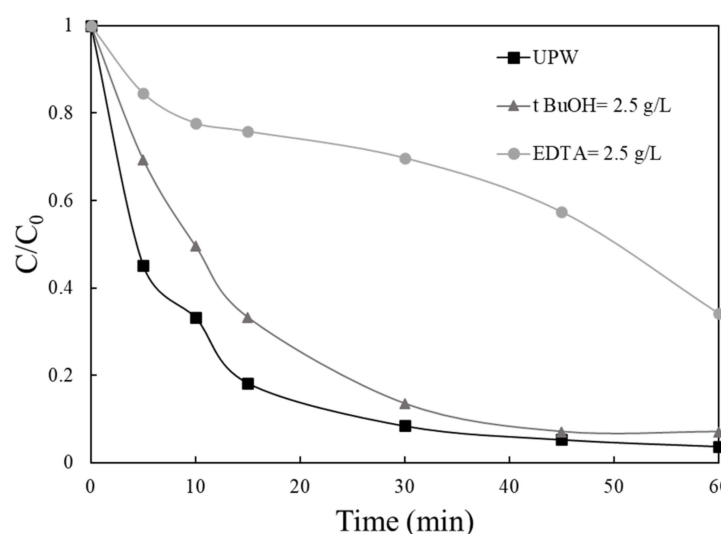
**Figure 10.** Effect of scavengers on the degradation of 0.5 mg/L VLS with 1000 mg/L 0.25 $MoS_2/BiOCl$.
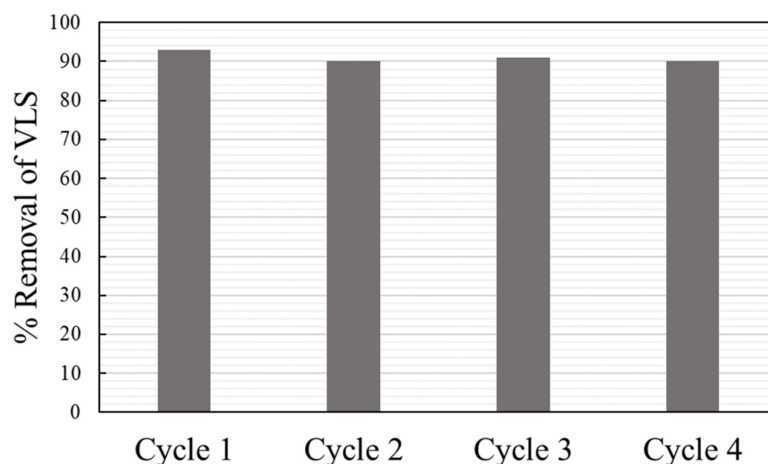


**Figure 11.** VLS removal for four consecutive runs using 0.25% $MoS_2/BiOCl$.

## 3. Materials and Methods

### 3.1. Chemicals and Water Matrices

Valsartan (VLS: $C_{24}H_{29}N_5O_3$) was obtained from the Pharmaceutical Department of the University of Patras. For catalyst preparation, bismuth (III) nitrate pentahydrate ($Bi(NO_3)_3 \cdot 5H_2O$), ammonium molybdate ($(NH_4)_2MoO_4$) and acetic acid ($CH_3COOH$) were supplied by Sigma-Aldrich. Ethylene glycol ($HOCH_2CH_2OH$, 99+%) and thiourea ($CH_4N_2S$, 99%) were supplied by Alfa Aesar and potassium chloride (KCl) was supplied by Merck. Sodium chloride (NaCl, CAS:7647-14-5), sodium bicarbonate ($NaHCO_3$, CAS:144-55-8) and humic acid (HA, CAS:1415-93-6) were purchased from Sigma-Aldrich (Saint Louis, MO, USA).

The main water matrix characteristics used in this study are: Ultrapure water (UPW) produced by a water purification system with resistivity 18.2 MΩ·cm at 25 °C, bottled water (BW) (pH = 7.7, 355 μS/cm conductivity, 237 mg/L $HCO_3^-$, 3.7 mg/L $Cl^-$, 7.8 mg/L $SO_4^{2-}$, 1.1 mg/L $NO_3^-$), secondary treated wastewater (WW) (pH = 8, 8.8 mg/L total organic carbon).

### 3.2. Preparation of Photocatalyst

$MoS_2/BiOCl$ composites in powder form were prepared by a deposition–precipitation method [39]. A pre-weighted amount of $MoS_2$ was dissolved in 100 mL ethylene glycol:UPW ($C_2H_4O$:UPW, 1:1 $v/v$ ratio). After that, 4.8 g of $Bi(NO_3)_3 \cdot 5H_2O$ was added in the

solution and left under stirring (solution A), whereas 0.7 g of thiourea was dissolved in 10 mL of UPW (solution B). After 10 min, solution B was added in solution A, followed by addition of 0.7 g KCl. Finally, 100 mL of acetic acid solution (2% *v/v*) was added dropwise into the system. The resulting mixture was left under vigorous stirring for 1 h at room temperature. The final product was separated by vacuum filtration and dried at 70 °C overnight. Composites with different mass ratios of $MoS_2$ to BiOCl were prepared by varying the amounts of $MoS_2$ in the starting solution, while keeping the content of BiOCl constant. The prepared photocatalysts are denoted in the following section as $x$MoS$_2$/BiOCl, where *x* is the mass ratio of $MoS_2$ to BiOCl.

Pure BiOCl was prepared using the same method but in the absence of $MoS_2$.

Pure $MoS_2$ was synthesized as follows [48]: 0.80 g of $(NH_4)_2MoO_4$ and 5.12 g of thiourea, $(NH_2)_2C=S$, were added in 45 mL of triply distilled water, with magnetic stirring until they dissolved. This solution was then transferred in a 120 mL stainless steel autoclave and heated at 200 °C for 16 h. The final product was separated by vacuum filtration and dried at 70 °C overnight.

### 3.3. Catalyst Characterization

The crystalline structure of the as prepared sample was studied with the use of a Bruker D8 Advance instrument with a Cu Ka source ($\lambda$ = 1.5496 Å, 10°–80°, scan rate of 0.05° s$^{-1}$, step size of 0.015°). Phase identification was based on JCPDS cards. The primary crystallite size of nanocrystals was estimated by means of the Debye–Scherrer's formula [49]. A UV–vis spectrophotometer (Varian Cary 3e) with an integrating sphere, using $BaSO_4$ as a reference, were used to obtain the diffuse reflectance spectrum of BiOCl. SEM images were recorded using a JEOL 6300 microscope equipped with an energy dispersive spectrometer (EDS) allowing elemental mapping of the photocatalytic material. The specific surface area of the sample was determined by means of nitrogen physisorption at the temperature of liquid nitrogen (77 K), (BET method), with the use of a Micromeritics Gemini III-2375 Surface Area Analyser. A Gatan model 782 ES500 W Erlangshen CCD camera was used for TEM analysis. A Malvern Zetasizer was used to conduct zeta potential measurements using laser Doppler micro-electrophoresis.

### 3.4. Experimental Procedure

In order to prepare the photocatalytic reactor (a Pyrex glass vessel), the desired amount of a stock VLS solution (65 mg/L) was added in UPW to achieve the desired initial SMX solution (0.5 mg/L in most cases). Then, the appropriate photocatalyst loading was added and the solution was left in the dark for 15 min to set up the absorption–desorption balance. A solar simulator (Oriel, model LCS-100, equipped with a 100 W xenon ozone-free lamp) provided the required radiation with an incident intensity equal to $7.3 \times 10^{-7}$ Einstein/(L.s) [47]. VLS degradation was monitored by high performance liquid chromatography (Waters Alliance 2695), as described elsewhere [22].

## 4. Conclusions

In the present work, a series of $MoS_2$/BiOCl composites with different $MoS_2$ mass ratios were tested for VLS photocatalytic removal. Summarizing:

- The addition of small amounts of $MoS_2$ on BiOCl enhanced its photocatalytic activity, which is maximized for the 0.25 wt.% $MoS_2$ sample.
- Several operating factors influence VLS degradation kinetics, such catalyst and VLS concentration and the water matrix.
- The organic matter present in real water matrices seem to slow down VLS removal rate.
- The photogenerated holes are proposed to be the primary oxidative species in the system.
- The as-synthesized 0.25 $MoS_2$/BiOCl photocatalyst exhibits excellent performance after repeated use.

## References

1. Kummerer, K. Antibiotics in the aquatic environment—A review—Part I. *Chemosphere* **2009**, *75*, 417–434. [CrossRef] [PubMed]
2. López-Pacheco, I.Y.; Silva-Núñez, A.; Salinas-Salazar, C.; Arévalo-Gallegos, A.; Lizarazo-Holguin, L.A.; Barceló, D.; Iqbal, H.M.N.; Parra-Saldívar, R. Anthropogenic contaminants of high concern: Existence in water resources and their adverse effects. *Sci. Total Environ.* **2019**, *690*, 1068–1088. [CrossRef] [PubMed]
3. Tran, N.H.; Reinhard, M.; Gin, K.Y.-H. Occurrence and fate of emerging contaminants in municipal wastewater treatment plants from different geographical regions—A review. *Water Res.* **2018**, *133*, 182–207. [CrossRef]
4. Martinez-Pachon, D.; Espinosa-Barrera, P.; Rincon-Ortiz, J.; Moncayo-Lasso, A. Treatment of two sartan antihypertensives in water by photo-electro-Fenton using BDD anodes: Degradation kinetics, theoretical analyses, primary transformations and matrix effects. *Chemosphere* **2021**, *270*, 129491. [CrossRef] [PubMed]
5. Rosario Brunettom, M.; Contreras, Y.; Clavijo, S.; Torres, D.; Delgado, Y.; Ovalles, F.; Ayala, C.; Gallignani, M.; Estela, J.J.; Martin, V.C. Determination of losartan, telmisartan, and valsartan by direct injection of human urine into a column-switching liquid chromatographic system with fluorescence detection. *J. Pharm. Biomed. Anal.* **2009**, *50*, 194–199. [CrossRef] [PubMed]
6. Saydam, M.; Takka, S. Bioavailability file: Valsartan. *FABAD J. Pharm. Sci.* **2007**, *32*, 185–196.
7. Hernández, F.; Ibáñez, M.; Gracia-Lor, E.; Sancho, J.V. Retrospective LC-QTOF-MS analysis searching for pharmaceutical metabolites in urban wastewater. *J. Sep. Sci.* **2011**, *34*, 3517–3526. [CrossRef] [PubMed]
8. Klosterhaus, S.L.; Grace, R.; Hamilton, M.C.; Yee, D. Method validation and reconnaissance of pharmaceuticals, personal care products, and alkylphenols in surface waters, sediments, and mussels in an urban estuary. *Environ. Int.* **2013**, *54*, 92–99. [CrossRef]
9. Seabra Pereira, C.D.; Maranho, L.A.; Cortez, F.S.; Pusceddu, F.H.; Santos, A.R.; Ribeiro, D.A.; Cesar, A.; Guimarães, L.L. Occurrence of pharmaceuticals and cocaine in a Brazilian coastal zone. *Sci. Total Environ.* **2016**, *548–549*, 148–154. [CrossRef]
10. Botero-Coy, A.M.; Martínez-Pachón, D.; Boix, C.; Rincón, R.J.; Castillo, N.; Arias-Marín, L.P.; Manrique-Losada, L.; Torres-Palma, R.; Moncayo-Lasso, A.; Hernández, F. An investigation into the occurrence and removal of pharmaceuticals in Colombian wastewater. *Sci. Total Environ.* **2018**, *642*, 842–853. [CrossRef]
11. Klavarioti, M.; Mantzavinos, D.; Kassinos, D. Removal of residual pharmaceuticals from aqueous systems by advanced oxidation processes. *Environ. Int.* **2009**, *35*, 402–417. [CrossRef]
12. Giwa, A.; Yusuf, A.; Balogun, H.A.; Sambudi, N.S.; Bilad, M.R.; Adeyemi, I.; Chakraborty, S.; Curcio, S. Recent advances in advanced oxidation processes for removal of contaminants from water: A comprehensive review. *Process Saf. Environ.* **2021**, *146*, 220–256. [CrossRef]
13. Parsons, S. *Advanced Oxidation Processes for Water and Wastewater Treatment*; IWA Publishing: London, UK, 2004.
14. Petala, A.; Noe, A.; Frontistis, Z.; Drivas, C.; Kennou, S.; Mantzavinos, D.; Kondarides, D.I. Synthesis and characterization of CoOx/BiVO4 photocatalysts for the degradation of propyl paraben. *J. Hazard. Mater.* **2019**, *372*, 52–60. [CrossRef] [PubMed]
15. Hapeshi, E.; Achilleos, A.; Vasquez, M.I.; Michael, C.; Xekoukoulotakis, N.P.; Mantzavinos, D.; Kassinos, D. Drugs degrading photocatalytically: Kinetics and mechanisms of ofloxacin and atenolol removal on titania suspensions. *Water Res.* **2010**, *44*, 1737–1746. [CrossRef]
16. Carp, O.; Huisman, C.L.; Reller, A. Photoinduced Reactivity of Titanium Dioxide. *Prog. Solid State Chem.* **2004**, *32*, 33–177. [CrossRef]
17. Lan, Y.; Lu, Y.; Ren, Z. Mini review on photocatalysis of titanium dioxide nanoparticles and their solar applications. *Nano Energy* **2013**, *2*, 1031–1045. [CrossRef]
18. Meng, X.; Zhang, Z. Bismuth-based photocatalytic semiconductors: Introduction, challenges and possible approaches. *J. Mol. Catal. A Chem.* **2016**, *423*, 533–549. [CrossRef]
19. Saison, T.; Chemin, N.; Chaneac, C.; Durupthy, O.; Mariey, L.; Mauge, F.; Brezova, V.; Jolivet, J.P. New Insights into BiVO4 Properties as Visible Light Photocatalyst. *J. Phys. Chem. C* **2015**, *119*, 12967–12977. [CrossRef]

20. Jiang, H.; Dai, H.; Meng, X.; Zhang, L.; Deng, J.; Liu, Y.; Au, C.T. Hydrothermal fabrication and visible-light-driven photocatalytic properties of bismuth vanadate with multiple morphologies and/or porous structures for Methyl Orange degradation. *J. Environ. Sci.* **2012**, *24*, 449–457. [CrossRef]

21. Nong, L.X.; Nguyen, V.H.; Bach, L.G.; Tran, T.V.; Nguyen, T.D. Photocatalytic activity for degradation of sulfamethoxazole by BiVO₄ using visible light. *IOP Conf. Ser. Mater. Sci. Eng.* **2020**, *736*, 042016. [CrossRef]

22. Ioannidi, A.; Petala, A.; Frontistis, Z. Copper phosphide promoted BiVO₄ photocatalysts for the degradation of sulfamethoxazole in aqueous media. *J. Environ. Chem. Eng.* **2020**, *8*, 104340. [CrossRef]

23. Park, Y.; McDonald, K.J.; Choi, K.-S. Progress in bismuth vanadate photoanodes for use in solar water oxidation. *Chem. Soc. Rev.* **2013**, *42*, 2321–2337. [CrossRef] [PubMed]

24. Zhang, K.L.; Liu, C.M.; Huang, F.Q.; Zheng, C.; Wang, W.D. Study of the electronic structure and photocatalytic activity of the BiOCl photocatalyst. *Appl. Catal. B Environ.* **2006**, *68*, 125–129. [CrossRef]

25. Wang, Y.; Deng, K.; Zhang, L. Visible light photocatalysis of BiOI and its photocatalytic activity enhancement by in situ ionic liquid modification. *J. Phys. Chem. C* **2011**, *115*, 14300–14308. [CrossRef]

26. Wei, Z.; Li, R.; Wang, R. Enhanced visible light photocatalytic activity of BiOBr by in situ reactable ionic liquid modification for pollutant degradation. *RSC Adv.* **2018**, *8*, 7956. [CrossRef]

27. Zhong, X.; Zhang, K.X.; Wu, D.; Ye, X.Y.; Huang, W.; Zhou, B.X. Enhanced photocatalytic degradation of levofloxacin by Fe-doped BiOCl nanosheets under LED light irradiation. *Chem. Eng. J.* **2020**, *383*, 132148. [CrossRef]

28. Ahmed, K.E.; Kuo, D.H.; Duresa, L.W. Synthesis and characterizations of BiOCl nanosheets with controlled particle growth for efficient organic dyes degradation. *J. Ind. Eng. Chem.* **2020**, *83*, 200–207. [CrossRef]

29. Chen, F.; Liu, H.; Bagwasi, S.; Shen, X.; Zhang, J. Photocatalytic study of BiOCl for degradation of organic pollutants under UV irradiation. *J. Photochem. Photobiol. A Chem.* **2010**, *215*, 76–80. [CrossRef]

30. Shen, T.; Shi, X.; Guo, J.; Li, J.; Yuan, S. Photocatalytic removal of NO by light-driven Mn₃O₄/BiOCl heterojunction photocatalyst: Optimization and mechanism. *Chem. Eng. J.* **2021**, *408*, 128014. [CrossRef]

31. Zhang, D.; Tan, G.; Wang, M.; Li, B.; Dang, M.; Wang, Y.; Zhang, B.; Ren, H.; Xia, A. The enhanced photocatalytic activity of Ag-OVs-(0 0 1) BiOCl by separating secondary excitons under double SPR effects. *Appl. Surf. Sci.* **2020**, *530*, 147228. [CrossRef]

32. Tao, S.; Sun, S.; Zhao, T.; Cui, J.; Yang, M.; Yu, X.; Yang, Q.; Zhang, X.; Liang, S. One-pot construction of Ta-doped BiOCl/Bi heterostructures toward simultaneously promoting visible light harvesting and charge separation for highly enhanced photocatalytic activity. *Appl. Surf. Sci.* **2021**, *543*, 148798. [CrossRef]

33. Liu, W.; Wang, S.; Zhao, Y.; Sun, C.; Xu, H.; Zhao, J. PVP-induced Bi₂S₃/BiOCl photocatalyst with open hollow structures for the removal of ciprofloxacin under visible-light irradiation. *J. Alloys Compd.* **2020**, 157995. [CrossRef]

34. Bao, S.; Liang, H.; Li, C.; Bai, J. A heterostructure BiOCl nanosheets/TiO₂ hollow-tubes composite for visible light-driven efficient photodegradation antibiotic. *J. Photochem. Photobiol. A Chem.* **2020**, *397*, 112590. [CrossRef]

35. Wu, D.; Wang, X.; Wang, H.; Wang, F.; Wang, D.; Gao, Z.; Wang, X.; Wu, F.; Jiang, K. Ultrasonic-assisted synthesis of two dimensional BiOCl/MoS₂ with tunable band gap and fast charge separation for enhanced photocatalytic performance under visible light. *J. Colloid Interface Sci.* **2019**, *533*, 539–547. [CrossRef]

36. Qiao, X.; Hu, F.; Hou, D.; Li, D. PEG assisted hydrothermal synthesis of hierarchical MoS₂ microspheres with excellent adsorption behavior. *Mater. Lett.* **2016**, *169*, 241–245. [CrossRef]

37. Jeong, N.; Kim, H.; Kim, W.; Choi, J.Y.; Hwang, K.; Nam, J.; Han, J.; Jwa, E.; Jeong, Y.C. Direct synthesis, characterization, and reverse electrodialysis applications of MoS₂ thin film on aluminum foil. *Mater. Charact.* **2020**, *164*, 110361. [CrossRef]

38. Guan, Y.; Wu, J.; Liu, Q.; Gu, M.; Lin, Y.; Qi, Y.; Jia, T.; Pan, W.; He, P.; Li, Q. Fabrication of BiOI/MoS₂ heterojunction photocatalyst with different treatment methods for enhancing photocatalytic performance under visible-light. *Mater. Res. Bull.* **2019**, *120*, 110579. [CrossRef]

39. Hou, J.; Dai, D.; Wei, R.; Wu, X.; Wang, X.; Tahir, M.; Zou, J.J. Narrowing the Band Gap of BiOCl for the Hydroxyl Radical Generation of Photocatalysis under Visible Light. *ACS Sustain. Chem. Eng.* **2019**, *7*, 16569–16576. [CrossRef]

40. Abellan, M.N.; Gimenez, J.; Esplugas, S. Photocatalytic degradation of antibiotics: The case of sulfamethoxazole and trimethoprim. *Catal. Today* **2009**, *144*, 131–136. [CrossRef]

41. Yan, H.; Liu, L.; Wang, R.; Zhu, W.; Ren, X.; Luo, L.; Zhang, X.; Luo, S.; Ai, X.; Wang, J. Binary composite MoS₂/TiO₂ nanotube arrays as a recyclable and efficient photocatalyst for solar water disinfection. *Chem. Eng. J.* **2020**, *401*, 126052. [CrossRef]

42. Guo, L.; Yang, Z.; Marcus, K.; Li, Z.; Luo, B.; Zhou, L.; Wang, X.; Du, Y.; Yang, Y. MoS₂/TiO₂ heterostructures as nonmetal plasmonic photocatalysts for highly efficient hydrogen evolution. *Energy Environ. Sci.* **2018**, *11*, 106–114. [CrossRef]

43. Teng, W.; Wang, Y.; Huang, H.; Li, X.; Tang, Y. Enhanced photoelectrochemical performance of MoS₂ nanobelts-loaded TiO₂ nanotube arrays by photo-assisted electrodeposition. *Appl. Surf. Sci.* **2017**, *425*, 507–517. [CrossRef]

44. Medinas, D.B.; Cerchiaro, G.; Trindade, D.F.; Augusto, O. The carbonate radical and related oxidants derived from bicarbonate buffer. *IUBMB Life* **2007**, *59*, 255–262. [CrossRef] [PubMed]

45. Hu, L.; Flanders, P.M.; Miller, P.L.; Strathmann, T.J. Oxidation of sulfamethoxazole and related antimicrobial agents by TiO₂ photocatalysis. *Water Res.* **2007**, *41*, 2612–2626. [CrossRef]

46. Liu, T.; Wang, L.; Lu, X.; Fan, J.; Cai, X.; Gao, B.; Miao, R.; Wang, J.; Lv, Y. Comparative study of the photocatalytic performance for the degradation of different dyes by ZnIn₂S₄: Adsorption, active species and pathways. *RSC Adv.* **2017**, *7*, 12292–12300. [CrossRef]

47.　Petala, A.; Frontistis, Z.; Antonopoulou, M.; Konstantinou, I.; Kondarides, D.I.; Mantzavinos, D. Kinetics of ethyl paraben degradation by simulated solar radiation in the presence of N-doped TiO$_2$ catalysts. *Water Res.* **2015**, *81*, 157–166. [CrossRef]

48.　Wang, F.; Li, G.; Zheng, J.; Ma, J.; Yang, C.; Wang, Q. Hydrothermal synthesis of flower-like molybdenum disulfide microspheres and their application in electrochemical supercapacitors. *RSC Adv.* **2018**, *8*, 38945. [CrossRef]

49.　Cullity, B.D.; Weymouth, J.W. Elements of X-ray diffraction. *Am. J. Phys.* **1957**, *25*, 394–395. [CrossRef]